Physicæ

Main patterns of the geomagnetic field: A case study using principal component analysis

Virginia Klausner,[1,2,3,*] Odim Mendes,[3,†] Margarete Oliveira Domingues,[3,‡] and Andres Reinaldo Rodriguez Papa[3,§]

[1] *Universidade do Vale do Paraíba - UNIVAP 12244-000 São José dos Campos, SP, Brazil*
[2] *National Institute for Space Research - INPE 12227-010 São José dos Campos, SP, Brazil*
[3] *National Observatory - ON 20921-400, Rio de Janeiro, RJ, Brazil*

The horizontal magnetic components observed by ground-based observatories belonging to the INTERMAGNET network have been used to analyze the global pattern of the geomagnetic field variation. The approach is based on the Principal Component Analysis method applied to magnetograms from 2000 to 2005. Quiet and disturbed days were geomagnetically distinguished. The pattern of the geomagnetic field variation fluctuates bewilderingly over time. In this work, we are interested in determining the geomagnetic field variability presenting in each principal component. The results suggest that the oscillation patterns of the first, second and third components could be explained respectively by the first one, two and three terms of the geomagnetic field spherical harmonic expansion. The principal components provide a meaningful way to appraise the overall space-time decomposition of the geomagnetic field.

I. INTRODUCTION

The geomagnetic field varies with space and time in a non-trivial way. As typical behavior, ground based magnetic measurements show a repetitive diurnal variation that corresponds to the geomagnetically quiet days. However, there are many varieties of irregular variations that occur over time, characterizing a disturbed field. Among the magnetic disturbances we have geomagnetic storms, so called by analogy with weather, which are of great interest because their effects in several human activities [1].

The intensity of the geomagnetic disturbance in each day is described by indices. There are different indices that can be used depending on the character and the latitude influences in focus. Kp, AE and Dst and their derivations are the most used geomagnetic indices. The Kp index is a number from 0 to 9 obtained as the mean value of the disturbance levels within 3-h interval observed at 13 subauroral magnetic observatories. The minutely AE index (sometimes 2.5 minute interval) is obtained by the H-component measured from the magnetic observatories located at auroral zones. The index most used in low and mid-latitudes is the Dst index. It represents the variations of the H-component due to changes of the ring current, see [2] for more details.

Ref. [3] analyzed the day-to-day variation of the geomagnetic field by using principal component analysis (PCA) to better understand the oscillations of the daily profile. He has found that these oscillations associated with principal components (PCs) were originated by ionospheric currents.

This work aims to analyze global patterns in the geomagnetic variations measured on the ground from 2000 to 2005. In other words, we will show the main variations of the geomagnetic field by using PCA to better understand the oscillations of the global profile. Also, we propose to associated these oscillations to the main characteristics of the geomagnetic field. Several observatories were chosen according to their geographical location in order to obtain a good representation of the magnetic behavior, and also, to examine how the magnetic effects during quiet and disturbed periods (geomagnetic storm) can affect the global space and time configuration features of the geomagnetic field. The observatory of Vassouras, Rio de Janeiro, Brazil, was included in our study to explore the influence of the SAMA (South Atlantic Magnetic Anomaly), and also, for better understanding of magnetospheric processes in this region.

The organization of this work is as follows: in Section II, a short description of the physics related to magnetic variations is presented; in Section III, the methodology is described; in Section IV, the magnetic dataset is presented; in Section V, the results are shown and discussed; and in Section VI, the conclusions are established.

II. THE PHYSICAL PHENOMENON

Under quiet solar wind conditions, a quasi-stationary magnetosphere current system is established surrounding the Earth. Primary electrical current systems are structured and linked preserving the well-known magnetic morphology [4]. Nevertheless, under disturbed solar plasma conditions, the magnetosphere is modified and those systems of currents are altered.

A great contribution to the magnetic variations comes from geomagnetic storms. The primary causes of geomagnetic storms at Earth are strong dawn-to-dusk electric fields associated with the passage of southward directed interplanetary fields, passing the Earth for sufficiently long intervals of time (more than 3 hours) and with significant intensity, larger than 10 nT. The solar wind energy transfer mechanism is the magnetic reconnection between the interplanetary magnetic field and the Earth's magnetic field [2]. The magnetic field is affected significantly by variations of the solar wind ram pressure, which produces changes in the magnetopause current. As a result of this process, there is an increase of the horizontal magnetic field component at mid-to-low latitudes, the so-called storm sudden commencement (SSC) [5]. The characteristic signature of a magnetic storm is a depression in

* virginia@univap.br
† odim@dge.inpe.br
‡ mo.domingues@lac.inpe.br
§ papa@on.br

the horizontal component of the Earth's magnetic field due to changes of the ring current [2]. An increase in the strength of the equatorial ring current due to the increase of the trapped magnetospheric particle population is the basic defining property of a geomagnetic storm.

The interaction between the solar wind and the interplanetary magnetic field (IMF) and the magnetosphere produces a complicated interrelated current system illustrated by magnetosphere currents, tail currents, ring currents, field-aligned currents, ionospheric currents and lower electric circuits with atmospheric discharges [5]. In other words, this interaction creates a great variety of complex processes, which generate geomagnetic activity.

At high latitudes, a large horizontal current flows in regions D and E of the auroral ionosphere, which is called auroral electrojet. During disturbed periods, these currents are intensified and their limits can extend beyond auroral regions. This expansion is mostly caused by enhanced particle precipitations and enhanced ionospheric electric fields [6]. At the magnetic equator, the additional variations of the horizontal component are related to the effect of equatorwards penetration of electric fields from the field-aligned current which enhance the eastward current in the E-layer of ionosphere, known as equatorial electrojet (EEJ) [7].

The effects of the SAMA have also to be considered as a magnetic contribution. The quasi-trapped particles in the inner radiation belt can sink to the SAMA, which is a global minimum in the Earth's total magnetic field intensity [8]. These particles can reach ionospheric heights. Ref. [9] verified variations on some ionospheric parameters measured by ionosonde at Cachoeira Paulista (Brazil). The processes which cause energetic electrons to precipitate in the atmosphere are: magnetospheric wave-particle interaction, lightning or artificially induced wave-particle interaction, drift-resonance interactions and wave-particle interactions generated by plasma instabilities [10]. Ref. [11] studied geomagnetic storms occurred in October and November, 2000 and they noticed that both continuous and impulsive pulsations in the H-component of the geomagnetic field at São Martinho da Serra (SMS) were enhanced due to particle precipitations in the SAMA region. Ref. [12] analyzed the magnitude of wavelet coefficients of the H-component of the geomagnetic field in the region under the SAMA influence and concluded that it was well correlated with the energetic particle fluxes (protons and electrons). They suggested that the precipitation of energetic particle in the SAMA is quite similar to the auroral zone, the SAMA can be thought as a "pseudo-auroral region".

All aforementioned features can be related to the magnetic records on the ground.

III. METHODOLOGY

In this section, we introduce briefly the concept of the PCA and its properties.

A. Principal Component Analysis

Among the several available methods of analysis, Principal Component Analysis (PCA) is a particularly useful tool in studying the temporal and spatial relationships within large quantities of geophysical data, see [13] and the references therein. PCA is used to decompose a time-series into its orthogonal component modes, the first of which can be used to describe the dominant patterns of variance in the time series [14]. Also, the PCA is able to reduce the original data set of two or more observed variables by identifying the significant information from the data.

PCs are the eigenvectors of the correlation matrix between the variables. Their form depend directly on the interrelationships existing within the data itself. The first PC is that linear combination of the original variables, which when used as a linear predictor of these variables, explain the largest fraction of the total variance. The second, third PC, etc., explain the largest parts of the remaining variance [14].

Consider M variables $x_m(t)$, which might represent the geomagnetic observations at M observatories as functions of time. Let these be observed at N times, $i = 1,2,3,...,n$. We can construct the $n \times m$ matrix as follows:

$$X = \begin{vmatrix} x_{1\,1} & \cdots & x_{1\,m} \\ \vdots & \ddots & \vdots \\ x_{n\,1} & \cdots & x_{n\,m} \end{vmatrix}. \tag{1}$$

The center of gravity of the m points is $\overline{x}$ where the ith coordinate is

$$\overline{x} = \frac{1}{m}\sum_{j=1}^{m} x_{i\,j}. \tag{2}$$

The points measured from their center of gravity, $v_{i\,j} = x_{i\,j} - \overline{x_{i\,j}}$, can be written

$$V = \begin{vmatrix} v_{1\,1} & \cdots & v_{1\,m} \\ \vdots & \ddots & \vdots \\ v_{n\,1} & \cdots & v_{n\,m} \end{vmatrix}. \tag{3}$$

Dividing the element $v_{i\,j}$ by the standard deviation s_i, we rewrite each element of V as:

$$v_{i\,j} = \frac{v_{i\,j}}{s_i}. \tag{4}$$

After, we compute the correlation matrix of the V matrix. The correlation matrix is a symmetric matrix, since the correlation of column i with column j is the same as the correlation of column j with column i.

$$C = \frac{1}{N}[V\,V^T]. \tag{5}$$

The Principal Components (PC) are obtained by solving an eigenvalue equation,

$$C\,\vec{e} = \lambda\,\vec{e}. \tag{6}$$

In this case, λ is an eigenvalue and $\vec{e}$ is an eigenvector.

As explained by [3], the interpretation of the eigenvectors and the eigenvalues can be described as follows: the eigenvectors are the normalized orthogonal basis in phase space, and also, the set of vectors of the new coordinate system in the space different from the coordinate system of the original variables; and the eigenvalues are the corresponding variance of the distribution of the projections in the new basis.

B. Visualization of the Principal Components

We have chosen to display the PCs as counter maps in order to represent the contribution of each PC in relation to the geographic longitude and latitude. The contour maps were done through a kriging interpolation method [15]. Because the magnetic observatories, and consequently the data, were irregularly distributed, some edge effects were produced. These unrealistic highs and lows contours were specially staged beyond the boundaries of the supplied data. To minimize these effects, the maps were mirrored (both North and South) and repeated (East and West) in order to avoid interpolation errors in regions with small amounts of data, such as the Southern Hemisphere.

Fig. 1 shows an example of the principal component visualization as a contour map. In this PCA analysis, we use the first PC values obtained for 2000. This map presents the 26 geographical locations of the magnetic observatories that were analyzed by PCA (based on the correlation matrix) to summarize the main patterns of variations in the dataset. In this map, the horizontal axis displays the geographical longitude between -180° to 180° and the vertical axis displays the geographical latitude between -90° to 90°. The color bar located at the right side of the contour map shows the PC values intervals. The color range of this contour map varies from -120 to 400 with a resolution of 20. The same color range was used in Figs. 2, 3 and 4.

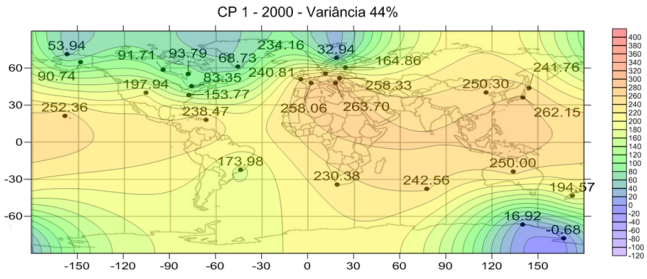

Figure 1: Example of the principal component visualization as a contour map.

IV. MAGNETIC DATA

The geomagnetic data used in this work relied on data collections provided by the INTERMAGNET programme [16]. We used hourly mean value series of the H geomagnetic component. Some magnetic observatories provide the X-component, in which case we have converted the X-component of the XYZ system to the H-component of the HDZ system [as described in 17]. We used $X = H\cos(D)$, where X is the northward component, H is the horizontal component and D is the angular direction of the horizontal component from the geographic north (declination). In principle, this system conversion does not affect our results because we are only interested in geomagnetic field variations.

Table I: INTERMAGNET network of geomagnetic observatories used in this study.

Station	IAGA code	Geographic coord.		Geomagnetic coord.	
		Lat.(^{o})	Long.(^{o})	Lat.(^{o})	Long.(^{o})
Scott Base (Antarctica)	SBA	-77.85	166.78	-78.97	-71.14
Eyrewell (New Zealand)	EYR	-43.42	172.35	-46.79	-106.06
Martin de Vivies (France)	AMS	-37.83	77.56	-46.07	144.94
Hermanus (South Africa)	HER	-34.41	19.23	-33.89	84.68
Alice Springs (Australia)	ASP	-23.76	133.88	-32.50	-151.45
Vassouras (Brazil)	VSS	-22.40	-43.65	-13.43	27.06
San Juan (Puerto Rico)	SJG	18.12	-66.15	27.93	6.53
Honolulu (United States)	HON	21.32	-158.00	21.59	-89.70
Kakioka (Japan)	KAK	36.23	140.18	27.46	-150.78
Fredericksburg (United States)	FRD	38.20	-77.37	48.40	-6.06
Boulder (United States)	BOU	40.13	-105.23	48.05	-38.67
Beijing (China)	BMT	40.30	116.20	30.22	-172.55
Memambetsu (Japan)	MMB	43.91	144.19	35.35	-148.23
Ottawa (Canada)	OTT	45.40	-75.55	55.63	-4.11
Hurbanovo (Slovakia)	HRB	47.87	18.19	46.87	101.17
Chambon la Foret (France)	CLF	48.02	2.26	49.56	85.72
Hartland (United Kingdom)	HAD	51.00	-4.48	53.88	80.17
Belsk (Poland)	BEL	51.83	20.80	50.05	105.18
Poste-de-la-Baleine (Canada)	PBQ	55.28	-77.75	65.48	-7.50
Brorfelde (Denmark)	BFE	55.63	11.67	55.45	98.22
Fort Churchill (Canada)	FCC	58.76	-94.09	67.58	-30.60
Nurmijarvi (Finland)	NUR	60.51	24.66	57.87	113.05
Narsarsuaq (Greenland)	NAQ	61.20	-45.40	69.91	38.58
College (United States)	CMO	64.87	-147.86	65.36	-97.23
Abisko (Sweden)	ABK	68.36	18.32	66.06	113.91
Barrow (United States)	BRW	71.32	-156.62	69.57	-112.56

Source: Ref. [18].

Both geomagnetically quiet and disturbed periods have been used, always considering data lengths of one year. We recognize as disturbed periods those days that presented Dst index < -30 nT. Using the hourly time resolution and the length of only one year, we removed the effects of the geomagnetic fields in high resolutions such as the induced telluric currents that vary from seconds to one hour period, and also, the long-term such as the secular variation. Also, all the INTERMAGNET magnetic observatories use standard instrumentation to produce standard data products which any contamination (such as might be caused by instrumentation faults or man-made interference) is removed from the data. The INTERMAGNET fundamental measurements are one-minute values of the vector components and of the scalar intensity of the field. The INTERMAGNET program calls for the world's magnetic observatories to be equipped with fluxgate and proton magnetometers (with a resolution of 0.1 nT) operating automatically under computer control. The INTERMAGNET dataset are one-minute values (data which have been corrected for baseline variations and which have had spikes removed and gaps filled where possible), with an absolute accuracy of ± 5 nT. For a full description see INTERMAGNET web site (`http://www.intermagnet.org`).

The corresponding IAGA codes and locations of the magnetic observatories used in this work are given in Table I in which the sequence is organized by the geographical latitude

of observatories. The choice of the 26 observatories followed some criteria such as: minimization of the number of gaps in the data, the maximum geographical distribution around the terrestrial globe and the availability of the magnetic observatory on the INTERMAGNET programme. These criteria also prioritize the magnetic observatory of Vassouras (VSS) and the validation of physical processes. However, some observatories have dataset gaps of the order of hours or even of some days. Before the analysis periods corresponding to these gaps were excluded from all the magnetic observatories. This exclusion does not affect the analysis, once the principal components represent the main modes of magnetic data oscillation.

V. RESULTS AND ANALYSIS

The PCs or "modes" for the 26 chosen magnetic observatories are presented as contour maps, as shown in Figs. 2 to 10. Each figure consists of 6 contour maps. Each map presents the global pattern of the geomagnetic field variation for the period between high (2000) and low solar activity (2005).

We choose the first three PCs because they reflect the major variations of the geomagnetic field, in other words, they represented the first three highest values of the series variances. Figs. 2, 5 e 8 (first, second and third components, respectively) show the geomagnetic field variations including both geomagnetically quiet and disturbed days.

We studied the period from 2000 to 2005. In the 6 contour maps, the PCs values kept the latitudinal symmetry and the location of its prevailing colors.

The first PC values including both geomagnetically quiet and disturbed days explained about 40% of the total magnetic series variance. From each eigenvalue λ_i of its corresponding $\vec{e}_i$, this percentage can be calculated from $100\,\lambda_i / \sum_{i=1}^{n} \lambda_i$. In other words, in PCA the eigenvalues describe how much the variance can be explained by its associated eigenvector.

Fig. 3, including only the quiet days, also shows latitudinal symmetry, however, the location of its prevailing colors changed. The yellow color region narrowed down to the equator region and the green and blue colors regions expanded from high to low latitudes.

However, only including geomagnetically quiet days, the first PC explained only about 25% of the total magnetic series variance.

In Fig. 4, just for the disturbed days, the latitudinal distribution of PCs values are quite similar to Fig. 2. In this figure, the highest PCs values (yellow) are located at the equator and low and middle latitudes, while the lower PCs values (green and blue) are located at regions of high latitudes.

Another similarity between Fig. 4 and Fig. 2 is that the first PC including only disturbed days also explained about 40% of the total magnetic series variance. Because of this similarity, it is possible to presume that the geomagnetic field disturbances have great influence on the first PCs variability.

Observing only the VSS observatory, it was found that this observatory eventually assumes a behavior similar to a low latitude observatories, and sometimes, to high latitude observatories. For example, in Fig. 2 (a, c, f), Fig.. 3 (a, b, c, d, e, f) and Fig. 4 (c e f) that represent the first PCA, and also, correspond to almost 50% of the H-component series variation, they presented the autovector value at VSS lower then the autovector values obtained at others geomagnetic observatories located at low and medium latitudes. On the other hand, observatories located at high latitudes presented lower values too, similar to VSS behavior. By this reason, this VSS behavior may be explained by its location, under the SAMA effect.

Likewise, regions with high intensity of the geomagnetic field had equivalent behavior. The total geomagnetic field is particularly high in the regions of Central Canada, Siberia and South of Australia and it is quite low near Southern Brazil [19]. It is possible to observe that the magnetic observatories, located at United States (BOU and FRD), China (BMT), Japan (KAK and MMB), Central Australia (ASP) and New Zealand (EYR), where the geomagnetic field is particularly high, presented similar behaviors.

Through a visual inspection, we compared the Figs. 2, 3 and 4 with the H-component IGRF-Applet maps [20]. All the visual inspection was carried out here in this paper was done using the H-component of the IGRF because it was the component used in all the dataset to calculated the PCs. Using only the first term on spherical harmonic expansion, we were able to analyze only the dipole influence of the geomagnetic field. The IGRF-Applet maps for the years from 2000 to 2005 also showed a latitudinal symmetry. The same latitudinal symmetry behavior was observed on Figs. 2, 3 and 4.

Therefore, the first principal component explains the influence due only to the dipole component of the geomagnetic field. Also, the first PCs values have a latitudinal dependence which is less pronounced considering only geomagnetically quiet days. This fact may be explained due to the ring current intensification during magnetic storms which causes a depression in the horizontal component detected by observatories located at low and middle latitudes.

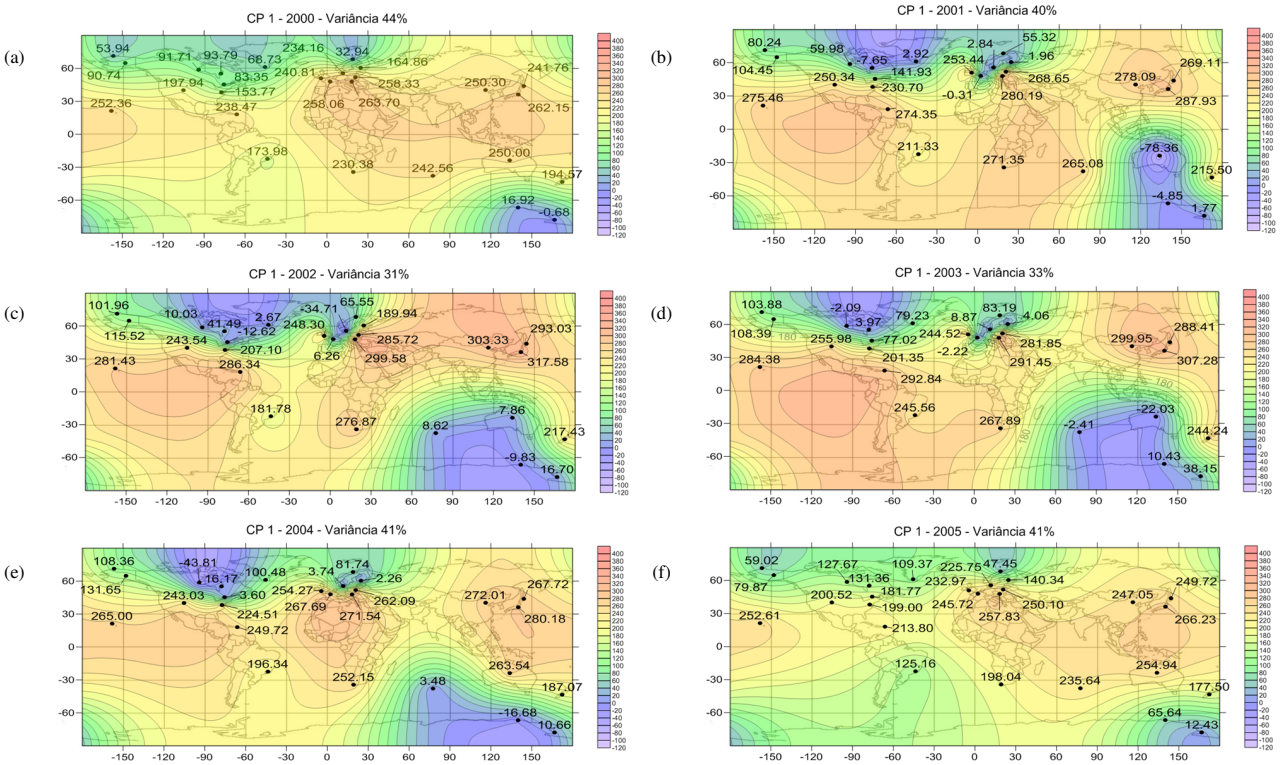

Figure 2: First mode of magnetic data oscillation including both quiet and disturbed periods for the years from (a) 2000 to (f) 2005.

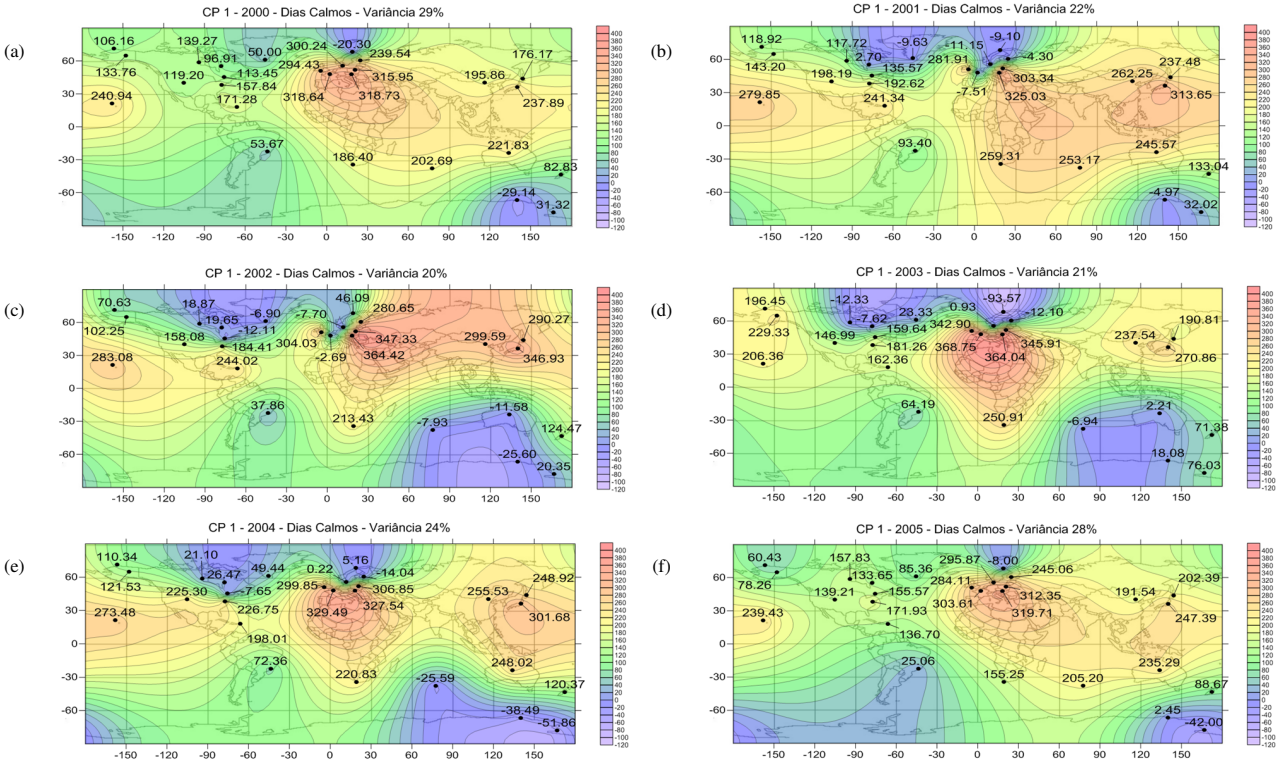

Figure 3: First mode of magnetic data oscillation including only quiet days for the years from (a) 2000 to (f) 2005.

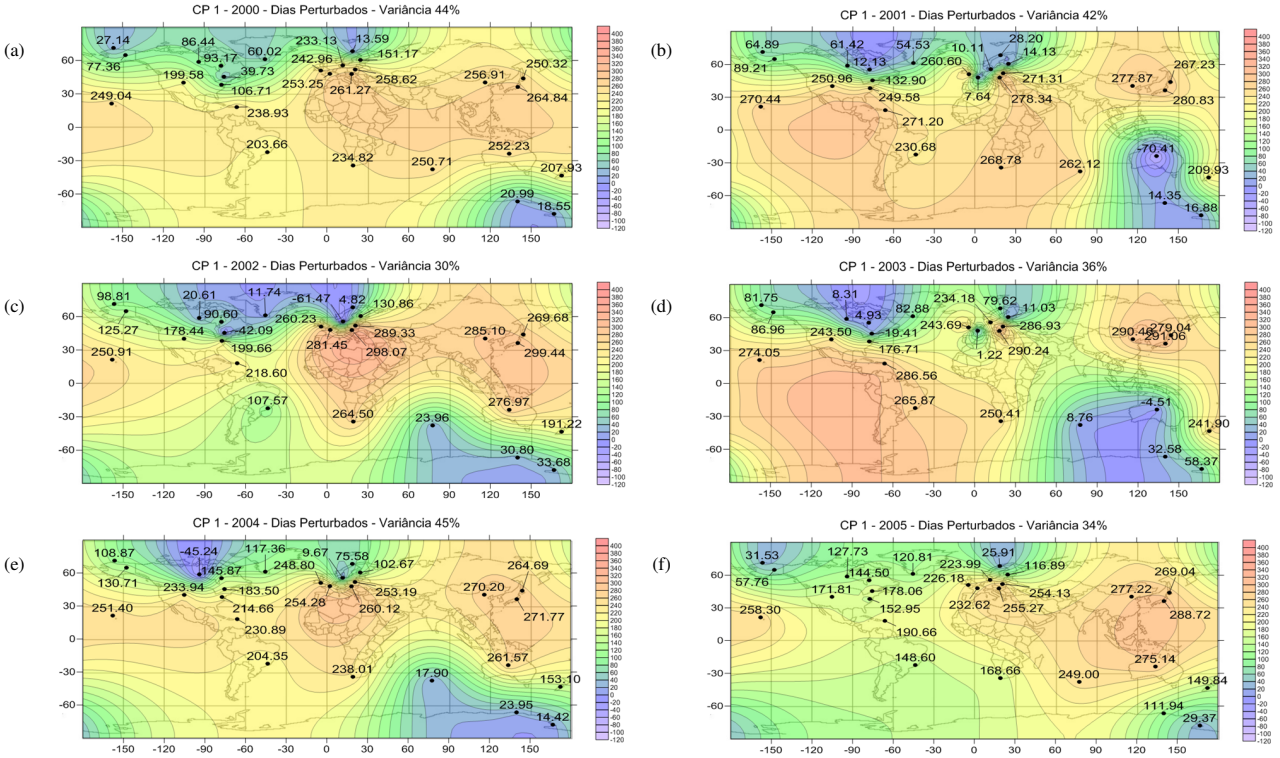

Figure 4: First mode of magnetic data oscillation including only disturbed days for the years from (a) 2000 to (f) 2005.

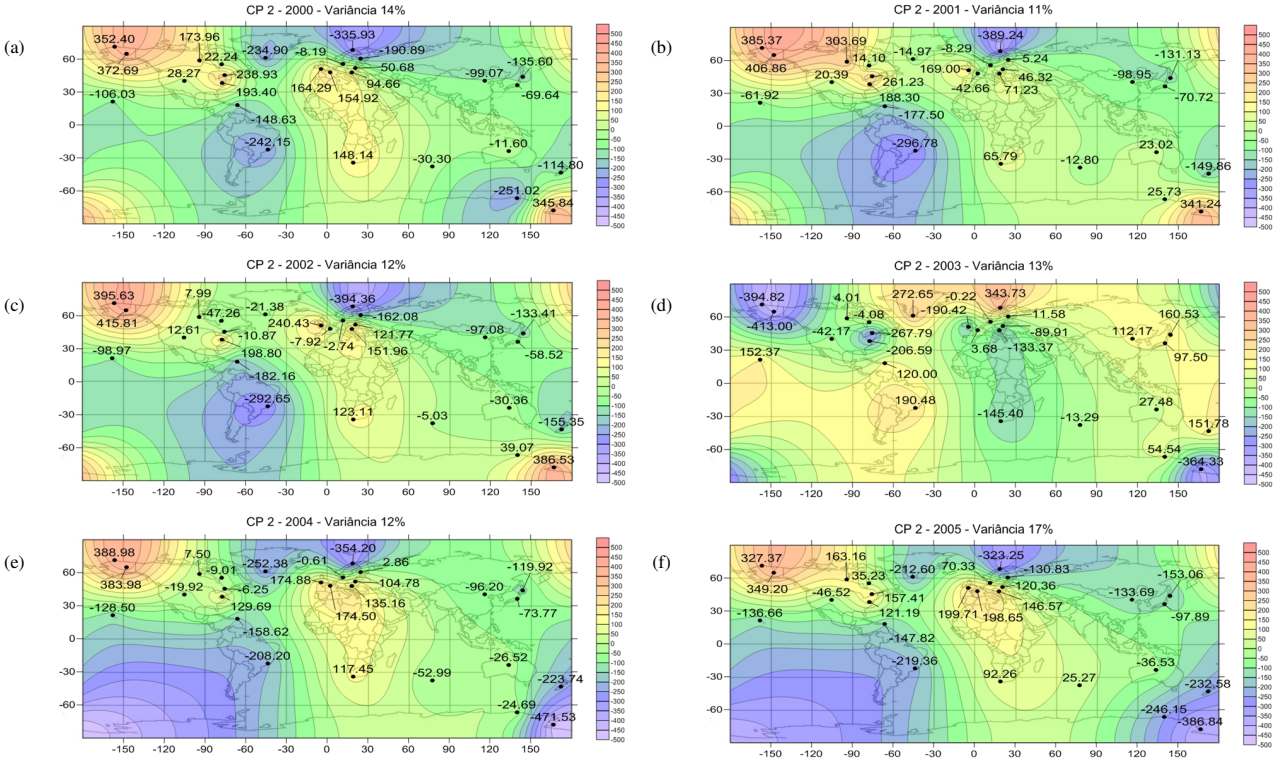

Figure 5: Second mode of magnetic data oscillation including both quiet and disturbed periods for the years from (a) 2000 to (f) 2005.

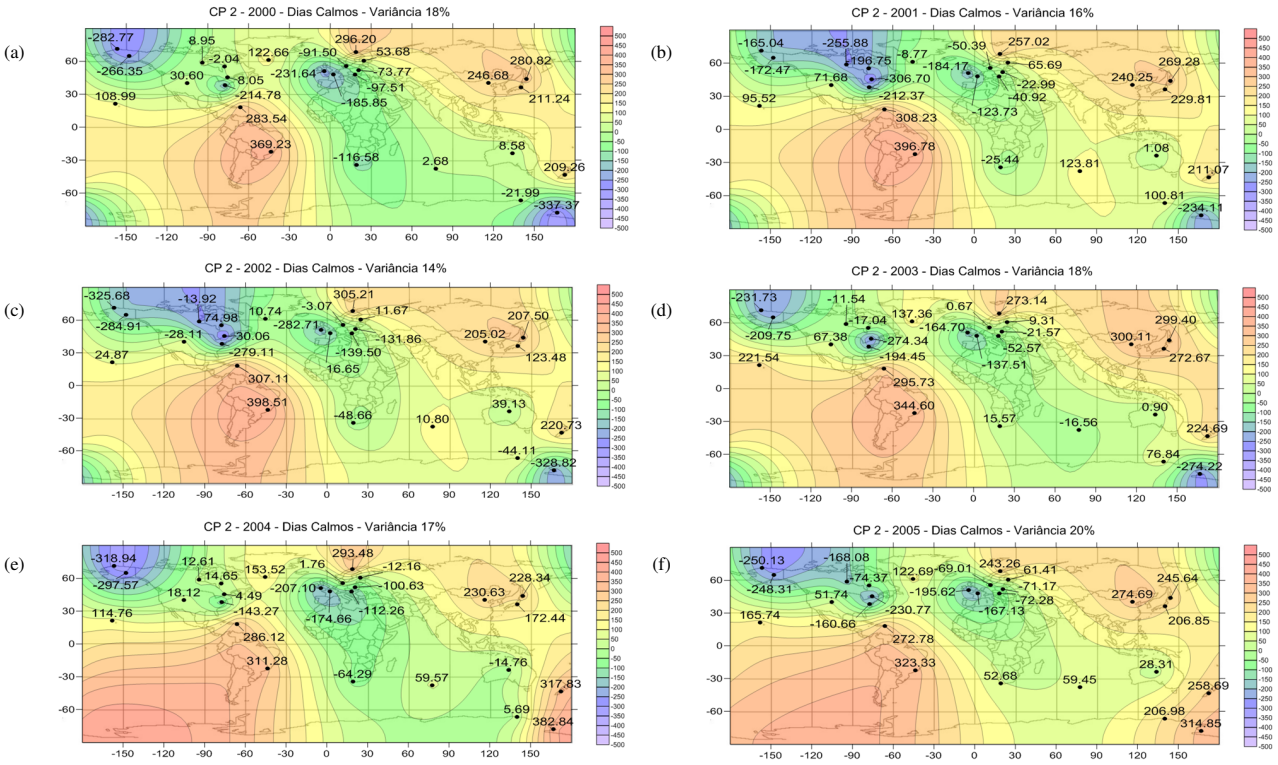

Figure 6: Second mode of magnetic data oscillation including only quiet days for the years from (a) 2000 to (f) 2005.

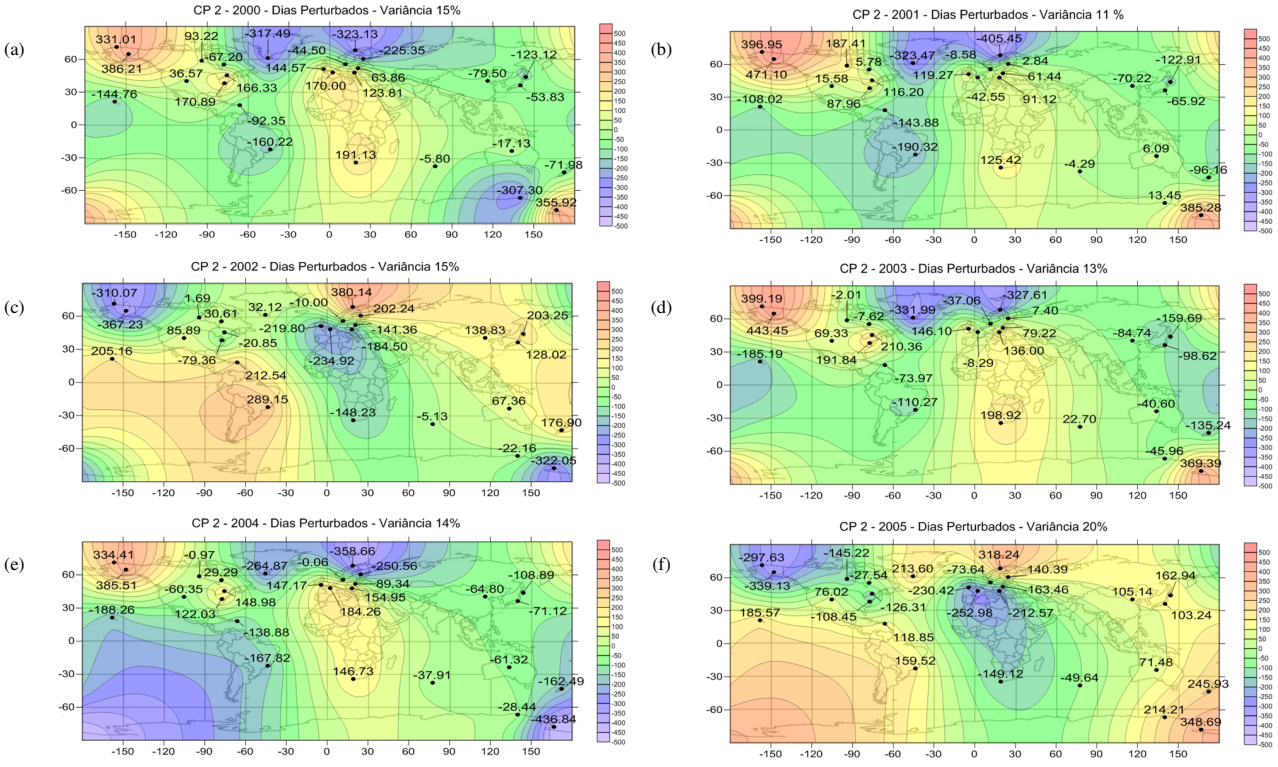

Figure 7: Second mode of magnetic data oscillation including only disturbed days for the years from (a) 2000 to (f) 2005.

Fig. 5 shows the pattern of second PC values distribution obtained at each magnetic observatory including both geomagnetically quiet and disturbed days. The color range of the 6 contour maps varies from -500 to 500 with a resolution of 50. The same color range was used in Figs. 6 and 7.

The contour maps of Fig. 5, except for the map of the year 2003, show two regions with maximum PCs values at North America and at Africa and some parts of the Asia, Australia and polar regions. These regions are represented in red and yellow colors which indicate the PCs values variation between 50 and 500.

On the other hand, the regions of minimum PCs values are located at Europe and at South America. These regions are represented in blue and purple which indicate PCs values variation between -500 and 0.

The contour map of the year 2003 presents the regions with minimum PCs values located at North America, at Africa and at the polar region. Meanwhile, the region of Europe and Greenland; and the region of South America, Russia and parts of Asia and Australia present the regions with maximum PCs values.

The second component accounted for about 13% of the total magnetic series variance.

Fig. 6 shows the second distribution pattern of PCs values including only geomagnetically quiet days. Unlike Fig. 5, the contour maps of Fig. 6 show the maximum PCs values at Central and South America, and also, at Asia. Meanwhile, the minimum PCs values appear at North America, West Europe and Africa. The second component including only geomagnetically quiet days accounted for about 17% of the total magnetic series variance.

Fig. 7 shows the second distribution pattern of PCs values including only disturbed days. The contour maps of the years 2000, 2001, 2003 and 2004 have distribution pattern of PCs values similar to the counter maps of Fig. 5. And contour maps of the years 2002 and 2005 similar to Fig. 6. The second component including only disturbed days accounted for about 15% of the total magnetic series variance.

By analyzing the Figs. 5, 6 and Fig. 7, the influence of magnetic disturbance is not a determining factor in the PCs value, nor in the percentage of the total magnetic series variance explained.

Once more, we compared the Figs. 5, 6 and 7 with the H-component IGRF-Applet maps. Using this time the first two terms on spherical harmonic expansion, we were able to analyze the dipole and quadrapole influence of the geomagnetic field. It can be observed that the distribution pattern of PCs values has well defined variation patterns at four distinct areas: Central and South America, Asia, Africa and North America. These patterns are similar to the geomagnetic field variation due to the influence dipole and quadrapole terms of the spherical harmonic expansion.

Fig. 8 shows the variation pattern of the third PC, including both the geomagnetically quiet days and disturbed days. The color range of the 6 contour maps varies from -600 to 600 with a resolution of 60. The same color range was used in Figs. 9 and 10. Comparing the Fig. 8 with the Figs. 2 and 5, this oscillation pattern is very distinct. The contour maps corresponding to years of 2000, 2003 and 2005 present the maximum of oscillation at three noticeable regions including: (1) Canada, Greenland and Western Europe; (2) Southern Australia and polar region; and (3) Hawaii. The minimum of oscillation is located mainly at South America.

The contour maps of 2001, 2002 and 2004 have the maximum and minimum of oscillations opposite to the regions described above.

The third PC including both quiet and disturbed magnetic days represents about 8% of the total magnetic series variance.

Fig. 9 shows the oscillation pattern of the third PC including only the geomagnetically quiet days. The contour maps for the years 2000, 2002, 2003, 2004 and 2005 present the maximum of oscillation located at: (1) Alaska; (2) United States Mid-West; and (3) South Africa, South America and polar region. While, the oscillation minimum are located at: (1) Canada and Greenland; (2) Hawaii; and (3) Australia and polar region. The contour map of 2001 has the oscillation pattern opposite to the maps described above.

This third PC explained about 10% of the total magnetic series variance.

Fig. 10 shows the oscillation pattern of the third PC including only the disturbed magnetic days. The contour maps for the years 2000, 2001 and 2004 are quite similar to the contour maps for the years 2000, 2003 and 2005 of Fig. 8. While the contour maps for the years 2002, 2003 and 2005 are similar to contour maps of Fig. 8 referring to 2001, 2002 and 2004.

This PC explains approximately 9% of the total magnetic series variance.

As occurred in the analysis of the second PC, comparing Fig. 8, 9 and 10 it can be said that the influence of magnetic disturbance is not a determining factor of the oscillation pattern, as well as on the percentage of the total magnetic series variance.

The pattern of H-component obtained by the IGRF-Applet maps using the first three terms on spherical harmonic expansion is quite similar to the oscillation pattern of Fig. 8, 9 and 10.

Therefore, the oscillation patterns of the third PCs can be explained due to the influence of the dipole, quadrapole and octapole components of geomagnetic field. Notwithstanding, this pattern is far more complicated than those of the first and second PCs.

This fact indicates the complexity of the currents system presented in ionosphere-magnetosphere system, even during quiet periods, because the influence of several phenomena such as solar activity, zenith angle of sunlight, geomagnetic storms, particles penetration and others. Also, the third component is less representative than the first and second PCs because it presents the lowest percentage of the total magnetic series variance.

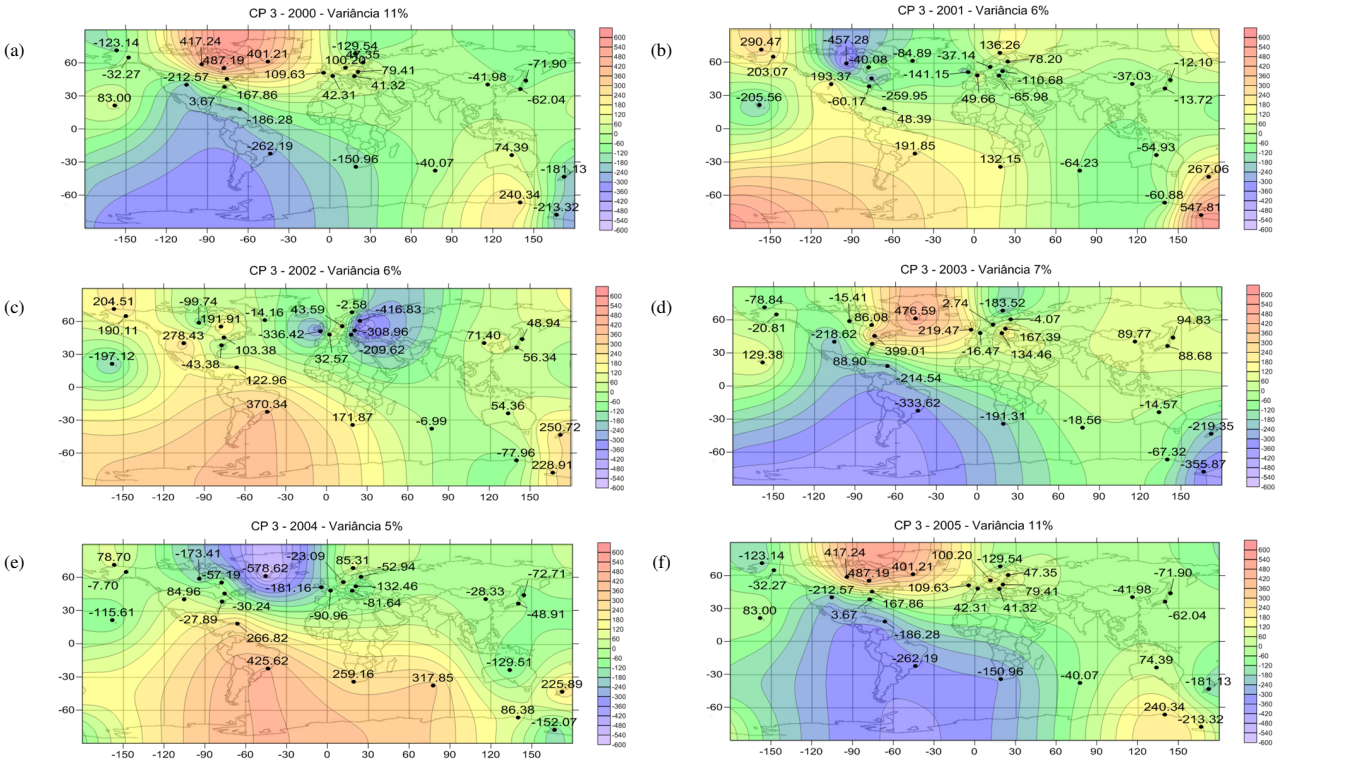

Figure 8: Third mode of magnetic data oscillation including both quiet and disturbed periods for the years from (a) 2000 to (f) 2005.

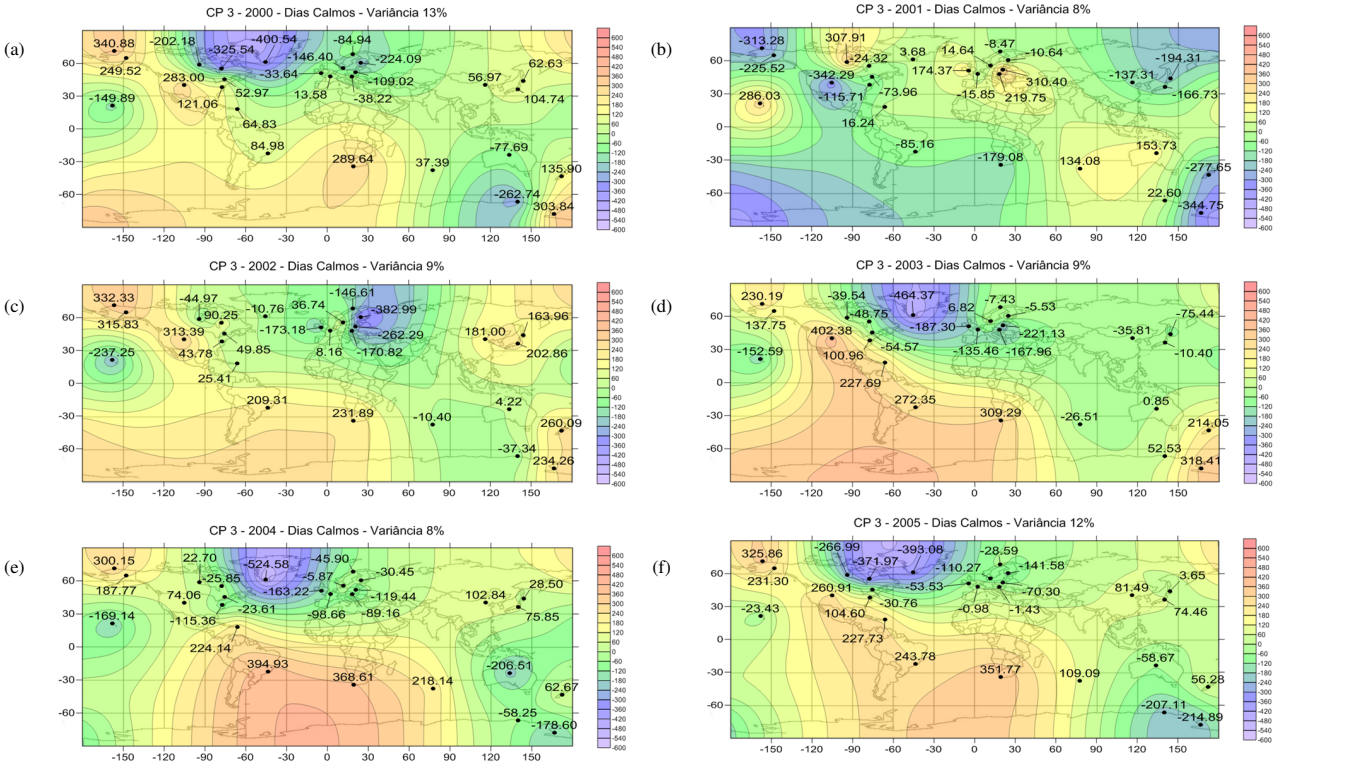

Figure 9: Third mode of magnetic data oscillation including only quiet days for the years from (a) 2000 to (f) 2005.

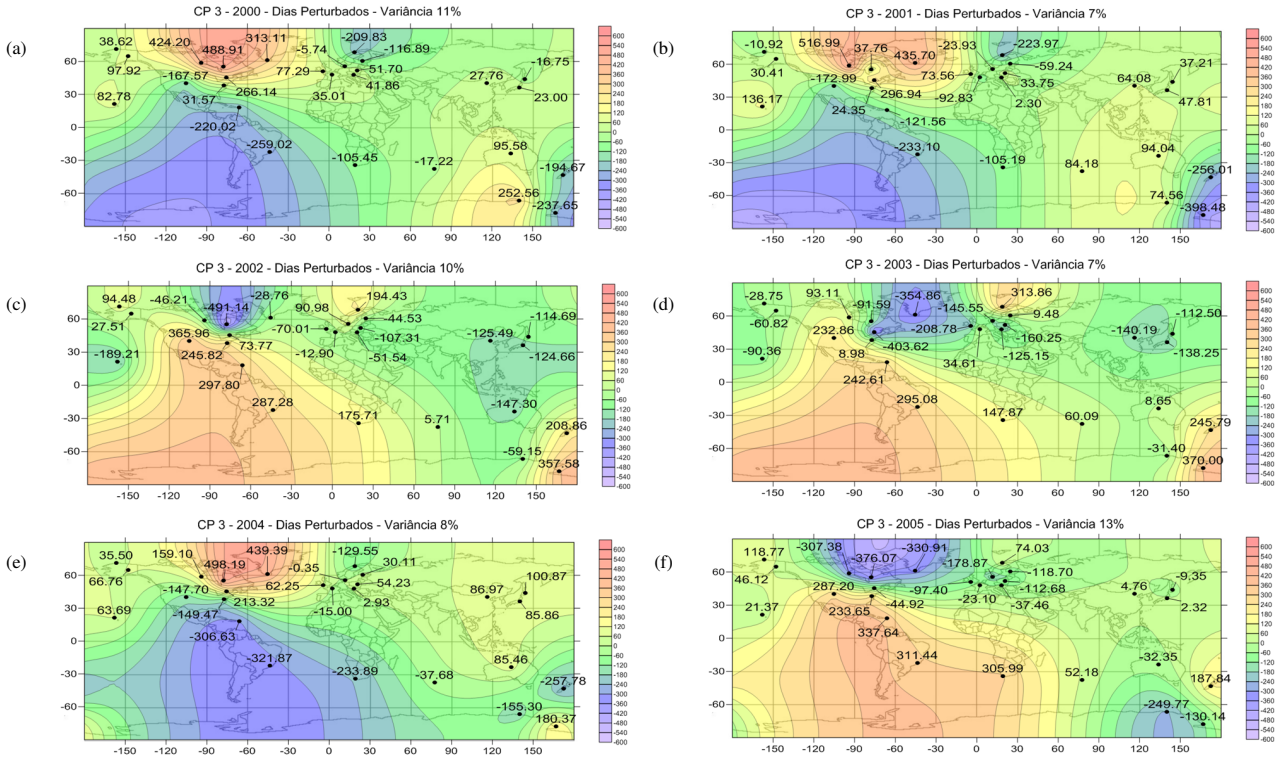

Figure 10: Third mode of magnetic data oscillation including only disturbed days for the years from (a) 2000 to (f) 2005.

VI. CONCLUSIONS

In this study, we evaluated the first three oscillation patterns of magnetic data. To process and analyze the magnetograms, we used the first three principal components obtained through the empirical orthogonal functions. This study made distinction between geomagnetically quiet and disturbed days.

The main results of this research are summarized as follows:

1. The variation of the first PC presented a latitudinal dependence. Although, this dependence is less pronounced when considered only geomagnetically quiet days, and enhanced when considered the disturbed days.

2. The first PC is mainly influenced by the dipolar component of the geomagnetic field.

3. The oscillation patterns of the second PCs can be explained by the influence of dipole and quadrapole components of the geomagnetic field.

4. The influence of magnetic disturbance is not a determining factor of the oscillation pattern, as well as on the percentage of the total magnetic series variance.

5. The third PCs patterns may represent the influence of dipole, quadrapole and octapole components of geomagnetic field.

6. In closing, the PCs provide a meaningful way to appraise the overall space-time decomposition of the geomagnetic field.

The PCA is an alternative technique to study the oscillation modes of geomagnetic data series due to it property of decomposing a time-series into its orthogonal component modes. As proposed here, we are able to decompose the geomagnetic field into its three dominant patterns of variance. This procedure is very similar to the spherical harmonical analysis. Using a network of magnetic observatories, we were able to divide the contributions of the geomagnetic field into dipole, quadrapole and octapole.

VII. ACKNOWLEDGMENTS

V. Klausner wishes to thanks CAPES for the financial support of her PhD (CAPES – grants 465/2008) and her Postdoctoral research (FAPESP – grants 2011/20588-7 and 2013/06029-0). The authors would like to thank the NOAA and the INTERMAGNET program for the datasets used in this work.

[1] W. D. Parkinson, *Introduction to Geomagnetism* (Scottish Academy Press, 1983) ISBN 9780707302928.
[2] Gonzalez, Journal of Geophysical Research: Space Physics **99**, 5771 (1994).
[3] Y. Yamada, Earth, Planets and Space **54**, 379 (2002).
[4] M. G. Kivelson and C. T. Russell, *Introduction to Space Physics*, Cambridge atmospheric and space science series (Cambridge University Press, 1995) ISBN 9780521457149.
[5] O. J. Mendes, A. Mendes da Costa, and M. O. Domingues, Advances in Space Research **35**, 812 (2005).
[6] I. A. Daglis and J. U. Kozyra, Journal of atmospheric and solar-terrestrial physics **64**, 253 (2002).
[7] L. Sizova, Advances in Space Research **30**, 2247 (2002).
[8] O. Pinto Jr. *et al.*, Journal of Atmospheric and Terrestrial Physics **54**, 1129 (1992).
[9] M. Nishino *et al.*, Earth, Planets and Space **54**, 907 (2002).
[10] O. Pinto Jr and W. D. Gonzalez, Journal of Atmospheric and Terrestrial Physics **51**, 351 (1989).
[11] N. B. Trivedi, B. M. Pathan, N. J. Schuch, M. Barreto, and L. G. Dutra, Advances in Space Research **36**, 2021 (2005).
[12] A. Mendes da Costa *et al.*, Journal of Atmospheric and Solar-Terrestrial Physics **73**, 1478 (2011).
[13] J. D. Horel, Journal of climate and Applied Meteorology **23**, 1660 (1984).
[14] C. W. Murray, J. L. Mueller, H. J. Zwally, and Goddard Space Flight Center, *Matrix partitioning and EOF/principal component analysis of Antarctic sea ice brightness temperatures* (National Aeronautics and Space Administration, Goddard Space Flight Center Greenbelt, Md, 1984) p. 1 v.
[15] M. A. Oliver and R. Webster, International Journal of Geographical Information Systems **4**, 313 (1990).
[16] "International Real-time Magnetic Observatory Network (INTERMAGNET)," (2015), `http://www.intermagnet.org`.
[17] W. H. Campbell, *Quiet Daily Geomagnetic Fields*, Pageoph Topical Volumes (U.S. Government Printing Office, 1989) ISBN 9783764323387, pp. 315–331.
[18] "World Data Center for Geomagnetism, Kyoto," (2015), `http://wdc.kugi.kyoto-u.ac.jp/igrf/gggm/index.html`.
[19] W. H. Campbell, *Introduction to Geomagnetic Fields* (Cambridge University Press, 1997) ISBN 9780521529532.
[20] "IGRF-Applet Maps," (2015), `http://www.ava.fmi.fi/MAGN/igrf/`.